ICARUS **125,** 233–244 (1997)
ARTICLE NO. IS965624

Separate Lightcurves of Pluto and Charon

MARC W. BUIE

Lowell Observatory, 1400 West Mars Hill Road, Flagstaff, Arizona 86001
E-mail: buie@lowell.edu

DAVID J. THOLEN

Institute for Astronomy, 2680 Woodlawn Drive, Honolulu, Hawaii 96822

AND

LAWRENCE H. WASSERMAN

Lowell Observatory, 1400 West Mars Hill Road, Flagstaff, Arizona 86001

Received December 9, 1994; revised August 26, 1996

We present new Hubble Space Telescope observations of the Pluto–Charon system taken with WFPC1 (PC6) between 1992 May 21 and 1993 August 18. Our observations consist of 52 images with the F555W filter and 8 images in the F439W filter. From these data we extracted individual lightcurves, phase coefficients, and colors for Pluto and Charon. These lightcurves have peak-to-peak variations of 0.33 and 0.08 mag, respectively. The lightcurve for Charon is consistent with its suspected synchronous rotation about Pluto. The linear phase coefficients are 0.0294 ± 0.0011 mag/deg for Pluto and 0.0866 ± 0.0078 mag/deg for Charon, spanning a range of phase angles from 0.6° to 2.0°. Charon's lightcurve has far less structure than Pluto's with minimum light corresponding to the anti-Pluto hemisphere. We found the $B-V$ color of Charon to be 0.710 ± 0.011 mag. Combined with previous mutual event measurements, the color of Charon is seen to be globally uniform. We also confirmed a reddish $B-V$ color for Pluto of 0.873 ± 0.002 and 0.862 ± 0.002 mag at 123° and 289° east longitude, respectively. These colors are consistent with prior mutual event observations but the higher precision measurement indicates that the surface of Pluto is slightly redder near minimum light.

INTRODUCTION

A full understanding of the planet Pluto cannot be achieved without first determining basic characteristics such as mass, size, shape, and albedo. Of these quantities, albedo has proved to be rather complicated, and a global average is insufficient if we are to understand the surface. Determination of the albedo distribution is quite difficult, due to Pluto's small angular size, though the large amplitude lightcurve provides an indication of considerable contrast. Understanding the albedo distribution through lightcurve data is further complicated by the photometric contribution of Charon. Although this contribution is only ~20% of the total flux, its effect cannot be ignored. Clearly, knowing the actual photometric contribution from Charon will help further the goal of determining the surface appearance of Pluto.

The mutual event season from 1984 to 1990 provided a new, powerful method of learning more about the individual properties of Pluto and Charon, including their relative albedos (cf., Tholen and Buie 1988, Buie *et al.* 1992, Young and Binzel 1993, Reinsch *et al.* 1994). Unfortunately, only at those few times when Charon was completely hidden from view could these data directly constrain their relative brightness. Due to the synchronous nature of the system, this constraint does not provide global information.

Other groundbased observations by Reitsema *et al.* (1983) and Jones *et al.* (1988) measured brightness ratios at opposite maximum elongations, which are 90° away from mutual event longitudes. However, these observations are isolated measurements that do not begin to characterize individual photometric properties. More recently, Olkin *et al.* (1993) obtained noisy individual lightcurves that suggested a smaller amplitude for Charon's lightcurve. Their observations were further hampered by essentially no phase angle coverage. Thus far, high-quality measurements of the individual lightcurves for Pluto and Charon have eluded even the best observatories in the world. While an isolated measurement might be possible on the best night at the best telescope from the ground, the slow rotation period requires this high quality on every night for a large number of nights. This combination of excellent quality

0019-1035/97 $25.00

nights combined with the need for adequate temporal coverage has proved difficult, if not impossible, to achieve.

The Hubble Space Telescope (HST), from its vantage point above our atmosphere, can easily resolve the Pluto–Charon system even in its aberrated, prerefurbishment condition. With this resolution, we can now measure the individual photometric properties of Pluto and Charon and thus provide a better starting point for future surface modeling of Pluto. Another advantage of working with HST is the much smaller time scheduling unit for observations, for which time is allocated by orbit (90 min) rather than by day. Thus it becomes possible to schedule and obtain the observations over the long time base required without an excessive allocation of observatory resources. This paper presents the photometric results from a systematic program we planned and executed on HST. An analysis of astrometric information from this dataset can be found in the companion paper by Tholen and Buie (1997).

OBSERVATIONS

Table I contains a log of our observations with the HST and the P6 chip of the WFPC1 instrument. The date, midtime, and filter is listed for each exposure. The F555W filter corresponds most closely to Johnson *V*, though the bandpass is quite a bit wider than the Johnson filter. The F439W filter most closely corresponds to a Johnson *B* bandpass. The columns labeled "Lat" and "Lon" are the latitude and longitude of the sub-Earth point in degrees. The column "Sep" is the measured separation between Pluto and Charon in pixels. The last three columns are the Sun–Pluto distance (AU), Earth–Pluto distance (AU), and the Sun–Pluto–Earth (phase) angle in degrees.

For each filter and epoch, we took images in pairs to provide some redundancy against cosmic ray strikes. The data collected between 1992 May 21 and 1993 July 06 were taken as originally planned. At the time of these images, Pluto was within ~20 arcsec of a star of similar brightness to Pluto. We expected to use the field star for a photometric, PSF, and astrometric reference object. The data taken between 1993 August 12 and 1993 August 18 are replanned observations replacing earlier observations that could not be executed due to the solar array drive electronics (SADE) failure and resulting spacecraft safing event of 1993 March 24. This failure led to a severe pointing restriction preventing observations near opposition. Given the additional timing constraints these latter data could not be scheduled at a time of a stellar appulse. Instead, we optimized the time of these observations to fill in gaps in our longitude coverage of the Pluto–Charon system.

We kept the exposure times fixed for all exposures at 30 sec for F555W and 120 sec for F439W. These exposure times were set to optimally expose Pluto while leaving sufficient margin for the lightcurve of Pluto to prevent saturation. We chose the F555W filter for the majority of the data because it is one of the best calibrated filters that can be transformed to a standard photometric system commonly used with Pluto photometry. A small number

TABLE I
Summary of Observations

UT Date	time	filter	Lat	Lon	Sep	r	Δ	α
1992/05/21	01:43:32.5	F555W	9.3	48.9	16.2	29.698	28.732	0.59
	01:49:32.5	F555W	9.3	48.6	16.1	29.698	28.732	0.59
	08:09:32.5	F555W	9.3	33.8	12.1	29.698	28.733	0.60
	08:15:32.5	F555W	9.3	33.5	12.1	29.698	28.733	0.60
1992/05/29	10:42:32.5	F555W	9.1	296.9	19.2	29.699	28.762	0.76
	10:48:32.5	F555W	9.1	296.7	19.4	29.699	28.762	0.76
	10:55:47.5	F439W	9.1	296.4	19.2	29.699	28.762	0.76
	11:04:47.5	F439W	9.1	296.1	19.2	29.699	28.762	0.76
	17:09:47.5	F439W	9.0	281.8	21.0	29.699	28.763	0.77
	17:18:47.5	F439W	9.0	281.4	21.0	29.699	28.763	0.77
	17:26:32.5	F555W	9.0	281.1	21.0	29.699	28.763	0.77
	17:32:32.5	F555W	9.0	280.9	21.0	29.699	28.763	0.77
1992/06/02	22:51:32.5	F555W	8.9	43.0	14.8	29.699	28.786	0.87
	22:57:32.5	F555W	8.9	42.8	14.7	29.699	28.786	0.87
1992/06/03	04:52:32.5	F555W	8.9	28.9	10.7	29.699	28.788	0.87
	04:58:32.5	F555W	8.9	28.6	10.6	29.699	28.788	0.87
1992/08/21	22:07:32.9	F555W	8.1	215.8	12.2	29.706	29.839	1.93
	22:13:32.9	F555W	8.1	215.5	12.2	29.706	29.839	1.93
1992/08/22	04:33:32.9	F555W	8.1	200.7	7.8	29.706	29.844	1.93
	04:39:32.9	F555W	8.1	200.4	7.7	29.706	29.844	1.93
1992/09/18	12:29:32.9	F555W	8.5	99.9	20.1	29.709	30.256	1.61
	12:35:32.9	F555W	8.5	99.7	20.1	29.709	30.256	1.61
	20:24:32.9	F555W	8.5	81.4	20.0	29.709	30.260	1.60
	20:30:32.9	F555W	8.5	81.1	20.0	29.709	30.260	1.60
1993/01/12	04:24:33.0	F555W	12.0	59.2	17.6	29.720	30.227	1.61
	04:30:33.0	F555W	12.0	58.9	17.6	29.720	30.227	1.61
	14:03:33.0	F555W	12.0	36.5	12.6	29.720	30.221	1.62
	14:09:33.0	F555W	12.0	36.3	12.6	29.720	30.221	1.62
1993/01/24	07:43:33.0	F555W	12.3	94.9	20.4	29.722	30.047	1.78
	07:49:33.0	F555W	12.3	94.7	20.4	29.722	30.047	1.78
	23:22:33.0	F555W	12.3	58.2	17.5	29.722	30.037	1.79
	23:28:33.0	F555W	12.3	57.9	17.5	29.722	30.037	1.79
1993/05/31	10:43:33.1	F555W	11.2	130.5	16.5	29.735	28.792	0.73
	10:49:33.1	F555W	11.2	130.3	16.6	29.735	28.792	0.73
	10:56:48.1	F439W	11.2	130.0	16.7	29.735	28.792	0.73
	11:05:48.1	F439W	11.2	129.7	16.8	29.735	28.792	0.73
	17:09:48.1	F439W	11.2	115.4	19.5	29.735	28.793	0.73
	17:18:48.1	F439W	11.2	115.1	19.6	29.735	28.794	0.74
	17:26:33.1	F555W	11.2	114.8	19.5	29.735	28.794	0.74
	17:32:33.1	F555W	11.2	114.5	19.6	29.735	28.794	0.74
1993/06/16	13:56:33.1	F555W	10.8	301.3	18.4	29.737	28.900	1.12
	14:02:33.1	F555W	10.8	301.1	18.4	29.737	28.900	1.12
	20:22:33.1	F555W	10.8	286.2	20.5	29.737	28.902	1.13
	20:28:33.1	F555W	10.8	286.0	20.5	29.737	28.902	1.13
1993/07/05	19:18:31.4	F555W	10.4	297.9	18.7	29.739	29.107	1.55
	19:24:31.4	F555W	10.4	297.7	18.8	29.739	29.107	1.55
1993/07/06	04:39:31.4	F555W	10.4	275.9	20.9	29.740	29.112	1.56
	04:45:31.4	F555W	10.4	275.7	20.9	29.740	29.112	1.56
1993/08/12	16:28:31.5	F555W	10.1	322.7	12.8	29.744	29.679	1.95
	16:37:31.5	F555W	10.1	322.4	12.9	29.744	29.679	1.95
1993/08/14	03:40:31.5	F555W	10.1	240.1	18.1	29.744	29.703	1.95
	03:49:31.5	F555W	10.1	239.7	18.1	29.744	29.703	1.95
1993/08/15	08:34:31.5	F555W	10.1	172.2	4.7	29.744	29.723	1.95
	08:44:31.5	F555W	10.1	171.8	4.6	29.744	29.723	1.95
	19:42:31.5	F555W	10.1	146.0	12.1	29.744	29.731	1.95
	21:18:31.5	F555W	10.1	142.3	13.0	29.744	29.732	1.95
1993/08/18	05:35:31.5	F555W	10.1	10.1	5.1	29.745	29.770	1.95
	05:44:31.5	F555W	10.1	9.7	4.9	29.745	29.771	1.95
	13:37:31.5	F555W	10.1	351.2	4.7	29.745	29.776	1.95
	13:46:31.5	F555W	10.1	350.9	4.8	29.745	29.776	1.95

of blue observations (F439W) were included to provide some additional constraint on the color of the objects.

The observations at each appulse consisted of two epochs of images separated by at least 6 hr. This time delay is sufficient to permit a significant rotation of Pluto (14°) and thus collect a distinct lightcurve measurement. The pair of observations becomes most important in the astrometric analysis of the data (see companion paper). We defined the "target" for HST to be the mid-point between the appulse star position and the geocentric position for the Pluto–Charon barycenter. The telescope was commanded to acquire and track the mid-point between the Pluto–Charon barycenter and the star while using the full on-board parallax correction for the distance to Pluto. This method generates a small smearing of the Pluto–Charon images and a slightly larger smear for the field star image. The makeup observations utilized simple blind pointing and tracking of the Pluto–Charon barycenter with the parallax correction.

We expected our photometry to be limited by calibration and other instrumental problems with HST, and we tried to devise an observing strategy that would minimize these difficulties. One particularly troublesome problem is occasional safing of the telescope that causes either a complete or partial shutdown of the spacecraft systems. In Cycles 1 and 2, any safing event led to a thermal change in the WFPC1 instrument, causing a change in the amount of contamination on the optics. These changes, in turn, create large shifts in the photometric zero-points of the instrument. The safing event itself actually causes additional material to be deposited on the optics. Part of the procedure of recovering from a safing involves removing these contaminants, but the amount removed never equals the amount deposited. To make matters worse, the contamination continually evolves between safing events, leading to a more gradual shift in zero-points with time. The full effect is usually an abrupt increase in system throughput upon recovery from a safing event followed by a period of gradual decrease in throughput in the weeks and months after safing. These drifts are seen as part of the photometric monitoring program (cf. MacKenty *et al.* 1993).

The field star in each image should have provided ample protection from the effects of safing on the absolute photometry. Groundbased photometric calibrations of these field stars should have allowed us to remove any zero-point drifts. Unfortunately, the flat field calibrations are not of sufficient accuracy to permit a useful flux extraction when the star and Pluto are on opposite sides of the CCD. The error is greatly reduced when comparing Pluto and Charon because the separation is always less than 1 arcsec. Thus we reduced and analyzed all of our imaging data without regard to the absolute flux levels measured by HST.

Our data were all taken with the early aberrated optics, and we had hoped to use the on-chip field star to provide a PSF reference for each image. However, the spatial variance in the aberrated PSF combined with the differing amounts of image smear was too large, precluding the use of the star as a PSF reference.

DATA REDUCTIONS

All data were reprocessed with the WFPC pipeline processing software in STSDAS version 1.3.1 as supplied by STScI. In general, the pipeline processing as provided on the original data tapes used old bias, dark, and preflash calibration frames. In particular, the preflash correction in the original pipeline processing does not account for the two different shutter blades used to illuminate the CCD. Each blade has a slightly different illumination pattern and the proper preflash calibration file must be used for each exposure. The best known calibration files as of April 1994 were selected from information provided by STScI and were used to run the pipeline processing.

Once the pipeline processing was completed, the images were further corrected by applying the appropriate delta flat to the image data. Delta flats are required to remove (for the most part) changes in the flat field that inevitably occur after every instrument safing event. This step removes most, but not all, of the persistent sensitivity variations (dubbed "measles" by STScI) in the image.

Ratnatunga *et al.* (1993) reported that generally available flat fields do not properly flatten the image and leave possibly large edge to edge sensitivity gradients. They have created better flat fields for the F555W filter, but similar work has not been done for the F439W filter. Even after applying this improved flat field, absolute photometry is no better than 3%. Photometry at this level is much worse than the state of the art for Pluto–Charon groundbased photometry (e.g., Tholen and Tedesco 1994, Binzel and Mulholland 1984, Reinsch *et al.* 1994). It may still be possible to improve the calibration of our data to permit absolute photometry by tying in the on-chip appulse stars, but the correction is sufficiently difficult and time consuming that we chose to use the groundbased observations of the system to calibrate the measurements. All the photometric results from our data will thus be confined to measuring the relative flux between Pluto and Charon. Given a maximum possible separation of 0.9 arcsec, the differential photometric errors should be quite small. Furthermore, because the observations are taken at random orbital longitudes, semirandom orientations on the CCD, and random locations on the CCD, any residual calibration errors should be manifest in the data as additional random scatter.

A direct extraction of the relative fluxes from the final calibrated images was not possible. The wings of the PSF from Pluto are much larger than the maximum distance to Charon. The PSF is far from symmetric and contami-

nates any small aperture flux that can be measured for Charon. This contamination varies strongly as Charon changes in its orbital position. Thus flux extraction requires removing the blurring effects of the aberrated PSF from each image.

We attempted three different image restoration techniques: Fourier deconvolution, maximum entropy restoration, and CLEAN. Of these three, only CLEAN provided a relatively easy mechanism for retaining full photometric accuracy in the restored images (Keel 1991). The CLEAN algorithm has its origin in radio astronomy where a known beam profile must be removed from the source signal (cf., Högbom 1974). This algorithm has been adapted by many to the optical domain provided by HST (e.g., Keel 1991). In simple terms, the algorithm assumes that the image is comprised of a collection of δ functions that have been convolved with some other known function (the PSF). Recovering the δ-function image requires an iterative approach. At each iteration, the peak absolute value of the image is located. At this location a PSF image is subtracted that has had its peak scaled to a fraction (called the gain) of the value of the peak in the image. The sum of the scaled PSF image is then added to a single pixel in an accumulator image at the location where the image extremum was found. For our data, we applied CLEAN to a 95 by 95-pixel subimage (4.1 arcsec wide) centered on Pluto with the search for the local extrema confined to within 1.3 arcsec of Pluto.

For best results, all cosmic ray strikes must be identified and removed. We used a combination of automatic and manual extraction methods to replace bad pixels by interpolating values from nearby pixels. Also, we removed the mean background signal local to the Pluto–Charon image prior to running CLEAN. This algorithm eventually converges in the sense that the amount subtracted from (or added to) the image approaches zero with an ever increasing number of iterations. If done properly, the original source image will be reduced to a random noise image with a mean of zero and the desired "cleaned" image will be contained in the δ-function image. The advantage of this process is that every photon collected in the source image is conserved and collected in the cleaned image.

In our case, we chose to use an iteration gain of 5%. Making the gain too large risks overcorrecting the image being cleaned. Making the gain too small changes the image too slowly and can require a larger number of iterations to get the same image restoration. We tested a few different gain values near 5% but the results never changed by much and 5% was fast enough for our dataset.

An important consideration in running CLEAN is having a good PSF to apply to the observed image. Our time allocation did not permit high-quality PSF observations closely spaced in time. Also, the on-chip appulse star is typically too far away in the focal plane to be used as a PSF reference. We attempted to use the PSF library provided in the HST archives at STScI. Unfortunately, the areal coverage over the 33-arcsec field-of-view of PC6 is poor as is the typical S/N level of the library PSF images. We achieved a better and more systematic match to our observed PSFs using numerical PSF images computed with a program provided by STScI named TinyTim version 2.4. This program can generate numerical PSF images at any image scale, source image color, and location on the CCD. In our experience, TinyTim provided good but not perfect PSF images when compared against observed PSF images.

We ran initial tests of the algorithm and image processing with 1000 iterations and the results were presented by Buie *et al.* (1994) at the 1994 Spring AGU meeting. Those results were enticing but of sufficiently low signal-to-noise ratio that a Charon lightcurve was not evident. Since that time we have analyzed the effect of iteration number on our results. At 1000 iterations, the *random* error in our differential photometry is several percent. Increasing the number of iterations to 10,000 greatly reduces the random error. The difference between 5000 and 10,000 iterations leads to random shifts in the flux *ratio* of 0.5%, which is well below other dominating noise sources. Our final results are based on 10,000 iterations of CLEAN with a gain of 0.05.

All output images from CLEAN were convolved with a Gaussian whose FWHM was 1.6 pixels (0.068 arcsec). This step performs a low-pass filter that removes all spurious high-frequency structure created by CLEAN and ensures the output image is properly sampled given the finite pixel size. The choice of FWHM = 1.6 pixels was dictated by the desire to have a sufficiently smoothed image that could be analyzed using normal techniques without smearing the image too much. We ran tests on synthetic Gaussian images, varying the FWHM, and found that widths smaller than 1.6 gave increasingly poorer centroided positions.

A representative sample of raw and CLEANed images is shown in Fig. 1. The images in the third column have been rotated to put north (J2000) at the top and are ordered by longitude to show the orbital motion of Charon. The images have all been scaled to the brightest pixel on Pluto. The relative brightness is preserved.

We used synthetic aperture photometry to extract the fluxes for each object. The numerical techniques used are described in detail in Buie and Bus (1992) and differ only in that the background is known to be zero and thus no additional background subtraction is done. An aperture radius of 3 pixels was chosen to return the maximum signal-to-noise ratio in the extracted photometry. The extracted flux is relatively insensitive to aperture centering errors as large as 0.5 pixels.

The relative flux measurements are listed in Table II. Tabulated are the original instrumental magnitudes as ex-

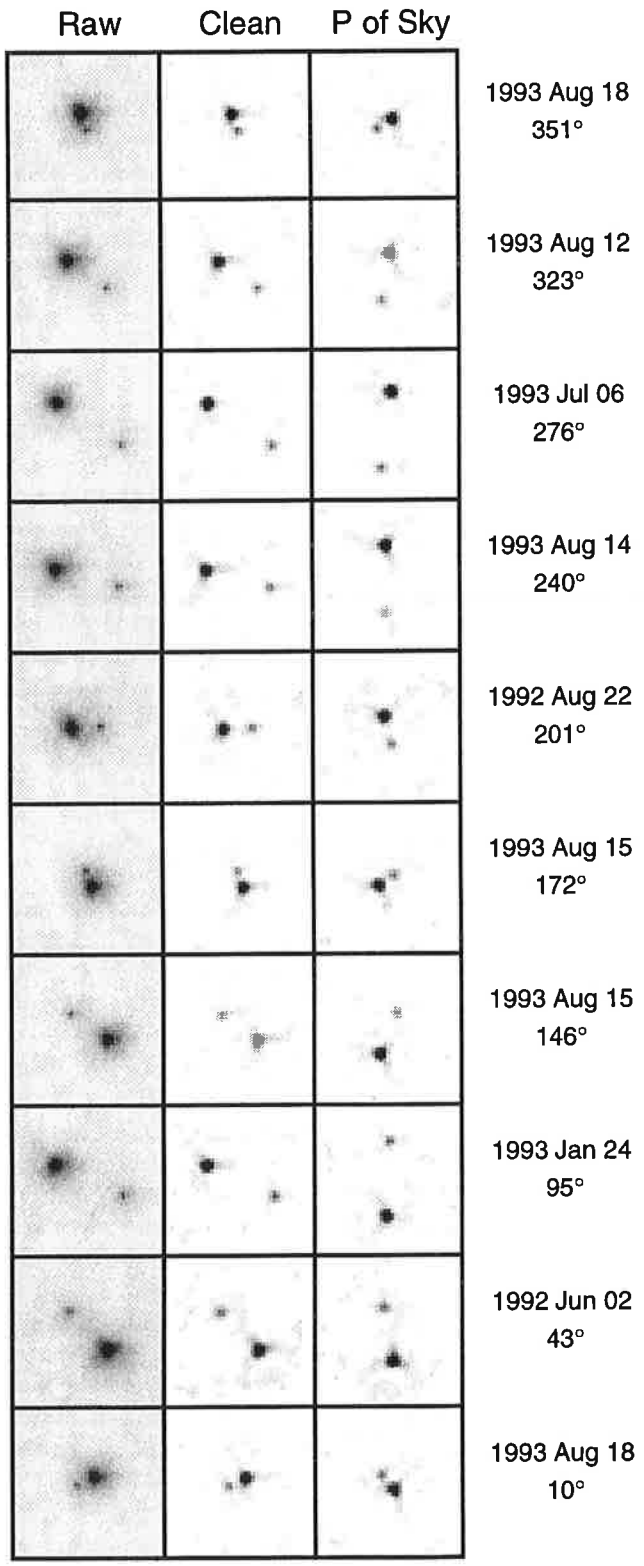

tracted from the image. At this stage, no attempt was made to transform these results to a standard system such as Johnson V, so only the relative values are important, not the absolute ones. The last column gives the magnitude difference between Charon and Pluto.

Before comparing these measurements to existing work on Pluto and Charon, the measurements must first be color corrected to the Johnson photometric system. Color corrections to the standard system were computed using the following equations from Harris *et al.* (1991),

$$(\mathrm{F439W} - B) = -0.0915(B - V) + 0.0168(B - V)^2 + Z_B,$$
$$(\mathrm{F555W} - V) = +0.0768(B - V) - 0.0254(B - V)^2 + Z_V. \quad (1)$$

This transformation is based on groundbased observations with a copy of the WFPC system and is expected to be the same as the on-orbit system. One test of this assumption was made shortly after the launch of HST. The results of the test were noisy, but there do not appear to be any significant differences between the on-orbit and groundbased systems (D. Hunter, private communication). We ignore the zero-points (Z_V and Z_B) because we use magnitude differences between Pluto and Charon only, thus canceling the zero-points. In transforming the data, we used the colors for Pluto and Charon as determined by Binzel (1988) where B–V is 0.867 for Pluto and 0.700 for Charon.

Our previous work in modeling the surface albedo of the Pluto–Charon system (Buie *et al.* 1992) resulted in a model that matches the observed lightcurve, including all effects from rotation, changing sub-Earth latitude, and solar phase angle. This model reproduces, to an accuracy of a few percent, the photometric record of the combined flux of Pluto and Charon over a baseline of 1954 to 1986. As such, our observations require a 6-year extrapolation for the lightcurve behavior at a time when the evolution of the lightcurve is known to be small (Tholen and Tedesco 1994, Reinsch *et al.* 1994). We believe our albedo model

FIG. 1. Sample of Pluto–Charon images. These images were all taken with the F555W filter. The left column of images is a 1.7-arcsec square extraction from the raw images centered on the mid-point between Pluto and Charon that still include the effects from the aberrated PSF. The center column is the resulting CLEANed image. These first two columns are in the original image orientation from the CCD. The right column (labeled P of Sky) shows the CLEANed image rotated so that J2000 north is toward the top of the image and east is to the left. The labels on the right indicate the day the image was taken and the sub-Earth longitude at that time. The orbital motion proceeds in increasing time from top to bottom. The satellite is clearly resolved even at minimum separation.

TABLE II
Instrumental Magnitudes for Pluto and Charon

Julian Date	Lon	filter	Pluto	Charon	Ch-Pl
2448763.57190	48.9	F555W	16.8410 ± 0.0014	18.7095 ± 0.0033	1.8685 ± 0.0036
2448763.57607	48.6	F555W	16.8658 ± 0.0014	18.6939 ± 0.0033	1.8281 ± 0.0036
2448763.83996	33.8	F555W	17.1352 ± 0.0016	18.9570 ± 0.0037	1.8218 ± 0.0040
2448763.84413	33.5	F555W	16.7438 ± 0.0013	18.5920 ± 0.0031	1.8482 ± 0.0034
2448771.94621	296.9	F555W	16.6371 ± 0.0013	18.6602 ± 0.0032	2.0231 ± 0.0035
2448771.95038	296.7	F555W	16.6764 ± 0.0013	18.6939 ± 0.0033	2.0175 ± 0.0035
2448771.95541	296.4	F439W	18.9087 ± 0.0015	20.8085 ± 0.0035	1.8999 ± 0.0038
2448771.96166	296.1	F439W	18.8942 ± 0.0015	20.7893 ± 0.0035	1.8951 ± 0.0038
2448772.21513	281.8	F439W	18.8793 ± 0.0014	20.7397 ± 0.0035	1.8604 ± 0.0038
2448772.22138	281.4	F439W	18.8810 ± 0.0014	20.7636 ± 0.0034	1.8826 ± 0.0037
2448772.22676	281.1	F555W	16.7644 ± 0.0013	18.7402 ± 0.0034	1.9758 ± 0.0036
2448772.23093	280.9	F555W	16.6973 ± 0.0013	18.7070 ± 0.0033	2.0098 ± 0.0036
2448776.45246	43.0	F555W	16.8331 ± 0.0014	18.7288 ± 0.0033	1.8957 ± 0.0036
2448776.45663	42.8	F555W	16.8544 ± 0.0014	18.7379 ± 0.0033	1.8835 ± 0.0036
2448776.70315	28.9	F555W	16.7002 ± 0.0013	18.6623 ± 0.0032	1.9621 ± 0.0035
2448776.70732	28.6	F555W	16.7286 ± 0.0013	18.6832 ± 0.0033	1.9546 ± 0.0035
2448856.42191	215.8	F555W	16.5744 ± 0.0012	18.6664 ± 0.0032	2.0920 ± 0.0035
2448856.42608	215.5	F555W	16.5736 ± 0.0012	18.6789 ± 0.0033	2.1053 ± 0.0035
2448856.68996	200.7	F555W	16.5922 ± 0.0012	18.5551 ± 0.0031	1.9629 ± 0.0033
2448856.69413	200.4	F555W	16.6062 ± 0.0013	18.5509 ± 0.0031	1.9447 ± 0.0033
2448884.02052	99.9	F555W	16.9636 ± 0.0015	18.7416 ± 0.0034	1.7780 ± 0.0037
2448884.02469	99.7	F555W	16.9708 ± 0.0015	18.7547 ± 0.0034	1.7839 ± 0.0037
2448884.35038	81.4	F555W	17.0042 ± 0.0015	18.7282 ± 0.0033	1.7240 ± 0.0037
2448884.35455	81.1	F555W	16.9991 ± 0.0015	18.7989 ± 0.0034	1.7998 ± 0.0038
2448999.68372	59.2	F555W	16.9131 ± 0.0014	18.8392 ± 0.0035	1.9261 ± 0.0038
2448999.68788	58.9	F555W	16.9118 ± 0.0014	18.8191 ± 0.0035	1.9072 ± 0.0038
2449000.08580	36.5	F555W	16.8021 ± 0.0014	18.7742 ± 0.0034	1.9721 ± 0.0037
2449000.08997	36.3	F555W	16.8138 ± 0.0014	18.8062 ± 0.0035	1.9924 ± 0.0037
2449011.82191	94.9	F555W	16.9736 ± 0.0015	18.7766 ± 0.0034	1.8029 ± 0.0037
2449011.82608	94.7	F555W	16.9582 ± 0.0015	18.7358 ± 0.0033	1.7775 ± 0.0036
2449012.47399	58.2	F555W	16.8486 ± 0.0014	18.7143 ± 0.0033	1.8656 ± 0.0036
2449012.47816	57.9	F555W	16.8395 ± 0.0014	18.7283 ± 0.0033	1.8888 ± 0.0036
2449138.94691	130.5	F555W	16.7459 ± 0.0013	18.5421 ± 0.0031	1.7963 ± 0.0033
2449138.95108	130.3	F555W	16.7336 ± 0.0013	18.5630 ± 0.0031	1.8294 ± 0.0034
2449138.95611	130.0	F439W	19.0794 ± 0.0016	20.7590 ± 0.0034	1.6796 ± 0.0038
2449138.96236	129.7	F439W	19.0941 ± 0.0016	20.7274 ± 0.0035	1.6333 ± 0.0038
2449139.21514	115.4	F439W	19.1090 ± 0.0016	20.6937 ± 0.0034	1.5847 ± 0.0037
2449139.22139	115.1	F439W	19.0965 ± 0.0016	20.7020 ± 0.0034	1.6054 ± 0.0038
2449139.22677	114.8	F555W	16.7787 ± 0.0014	18.5187 ± 0.0030	1.7400 ± 0.0033
2449139.23094	114.5	F555W	16.7713 ± 0.0014	18.5297 ± 0.0030	1.7584 ± 0.0033
2449155.08094	301.3	F555W	16.7040 ± 0.0013	18.7296 ± 0.0033	2.0256 ± 0.0036
2449155.08511	301.1	F555W	16.7222 ± 0.0013	18.7129 ± 0.0033	1.9907 ± 0.0036
2449155.34899	286.2	F555W	16.6314 ± 0.0013	18.5917 ± 0.0031	1.9603 ± 0.0034
2449155.35316	286.0	F555W	16.6345 ± 0.0013	18.6433 ± 0.0032	2.0088 ± 0.0035
2449174.30453	297.9	F555W	16.6951 ± 0.0013	18.7412 ± 0.0034	2.0461 ± 0.0036
2449174.30870	297.7	F555W	16.7017 ± 0.0013	18.7691 ± 0.0034	2.0674 ± 0.0037
2449174.69411	275.9	F555W	16.6113 ± 0.0013	18.6654 ± 0.0032	2.0541 ± 0.0035
2449174.69828	275.7	F555W	16.6246 ± 0.0013	18.6468 ± 0.0032	2.0222 ± 0.0035
2449212.18648	322.7	F555W	16.6252 ± 0.0013	18.6885 ± 0.0033	2.0633 ± 0.0035
2449212.19273	322.4	F555W	16.6253 ± 0.0013	18.7001 ± 0.0033	2.0749 ± 0.0035
2449213.65314	240.1	F555W	16.5094 ± 0.0012	18.6128 ± 0.0032	2.1034 ± 0.0034
2449213.65939	239.7	F555W	16.5115 ± 0.0012	18.6228 ± 0.0032	2.1113 ± 0.0034
2449214.85731	172.2	F555W	16.5859 ± 0.0012	18.4250 ± 0.0029	1.8391 ± 0.0032
2449214.86425	171.8	F555W	16.5908 ± 0.0012	18.4435 ± 0.0029	1.8527 ± 0.0032
2449215.32120	146.0	F555W	16.7160 ± 0.0013	18.6182 ± 0.0032	1.9022 ± 0.0034
2449215.38786	142.3	F555W	16.7428 ± 0.0013	18.5928 ± 0.0031	1.8500 ± 0.0034
2449217.73300	10.1	F555W	16.6512 ± 0.0013	18.5998 ± 0.0031	1.9486 ± 0.0034
2449217.73925	9.7	F555W	16.6584 ± 0.0013	18.5130 ± 0.0030	1.8546 ± 0.0033
2449218.06773	351.2	F555W	16.6416 ± 0.0013	18.4657 ± 0.0030	1.8241 ± 0.0032
2449218.07398	350.9	F555W	16.6505 ± 0.0013	18.5115 ± 0.0030	1.8610 ± 0.0033

can be trusted for any calculation involving the combined brightness of the Pluto–Charon system in either B or V as a function of solar phase angle or sub-Earth longitude.

Fortunately, our new dataset is very complementary to the groundbased data and the albedo model. From the albedo model we computed the combined magnitude, which accounts for all the geometry (solar phase angle, longitude) at the time of each observation. Figure 2 shows the model magnitudes for each of the F555W observations. The two sets of points show the model without phase correction and the model after the phase coefficient of Tholen and Tedesco (1994) is used.

Using the color of Binzel (1988), we converted the model magnitude from Johnson B to Johnson V (if needed). This step should have introduced relatively little error since the Reinsch *et al.* (1994) observations clearly show no change in the color of the system as a function of orbital longitude. Given the transformed relative magnitudes for Charon–Pluto, we can then compute the Johnson B and V magnitudes for Pluto and Charon individually.

ANALYSIS

Determining a final lightcurve for each of Pluto and Charon requires finding the phase coefficient. We used a technique very similar to that in Tholen and Tedesco (1994), which employs an n-term Fourier series fit simultaneously with a linear phase coefficient. We did not allow for a time dependent term in the fitting of the photometry due to the short time baseline of the observations. We also did not fit for a rotational period since we assumed the geometry to be known. The magnitude function we used is given by

$$V(\alpha, \lambda) = \sum_{n=0}^{M} (a_n \cos n\lambda + b_n \sin n\lambda) + \beta\alpha, \qquad (2)$$

where $V(\alpha, \lambda)$ is the Johnson V magnitude at the mean opposition distance of $r = 39.5$ AU and $\Delta = 38.5$ AU, α is the phase angle, λ is the sub-Earth longitude on Pluto at the time of observations, a_n and b_n are the coefficients to the Fourier series, M is the maximum order of the Fourier series fitted to the data, and β is the linear phase coefficient.

A linear least squares fit to the data was used to determine the Fourier coefficients and the phase coefficient. The geometry of the observation is assumed known and is calculated with the same ephemeris used for the albedo maps of Buie *et al.* (1992). While fitting the data for each object, the number of terms (M) was increased until the new terms added were no longer significant and the reduced χ^2 increased. Just as for the Tholen and Tedesco (1994) results, we found $M = 4$ worked best to fit the lightcurve of Pluto. The data for Charon do not show as much structure and are also more noisy, so $M = 2$ sufficed to provide a good fit to the photometry.

Eight points out of the total sample of 60 measurements had to be excluded from the fit. All of the Charon measurements near minimum separation are systematically higher than the rest of the photometry. Six of the eight points had overlapping photometric apertures and the other two were very close to overlapping. The error for these points is clearly caused photometric contamination between aper-

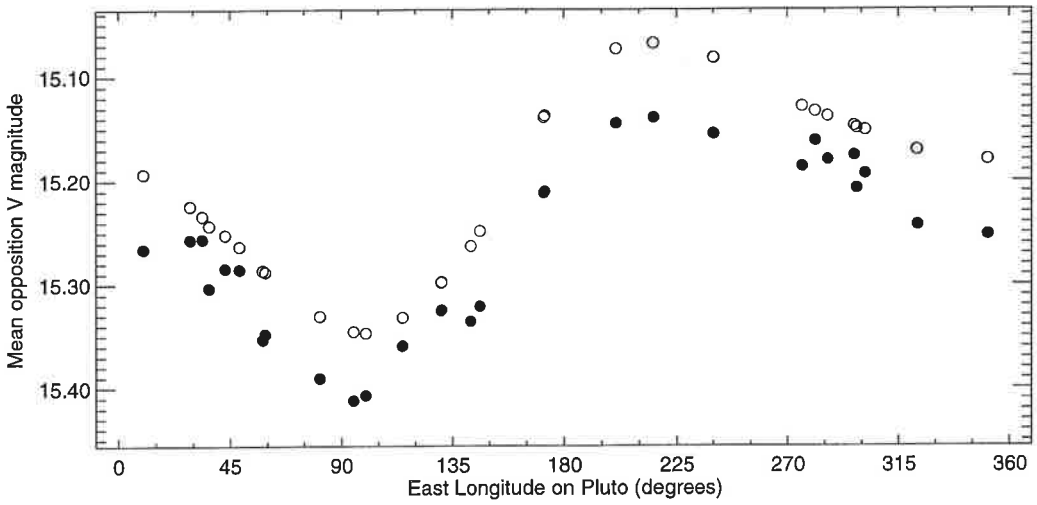

FIG. 2. Model Pluto+Charon magnitude. The filled circles are the direct result of the model calculation and include the photometric effects of the varying solar phase angle. The open circles show the model after removing the phase variation with the linear phase coefficient as determined by Tholen and Tedesco (1994) and is shown purely for illustrative purposes.

tures and would cause the flux ratio to be underestimated, thus making the inferred magnitude for Charon too bright. In fitting the data, all measurements within 15° of the minimum separation (0° and 180°) were excluded for both Pluto and Charon. The errors in the Pluto magnitudes are much smaller but still noticeable.

It was not feasible to make exhaustive test of the choice of PSF on the photometry. However, since the images are done at "random" times and chip locations, it is unlikely that a large, unrecognized source of systematic error exists. Instead, we might expect inflated random errors if our choices were not optimal. In the end, the internal consistency of the extracted photometry gave us reason to trust the process. Of all the measurements, the minimum separation data are the most sensitive to the choice of PSF but these were excluded from further analysis.

The resulting rotational lightcurves for Pluto and Charon are shown in Figs. 3 and 4, respectively. For these plots, the phase angle effects have been removed, leaving just the rotational modulation to the lightcurve. The phase functions for each object are seen by removing the rotational modulation and are shown in Figs. 5 and 6. The coefficients to the fitting functions are given in Tables III and IV. Also listed are the values for $\chi^2_{\rm red} = \chi^2/(N - f)$, where N is the number of data points and $f = 2M + 2$ is the number of degrees of freedom. The scatter in the fit $\overline{|O - C|}$ is also shown. For comparison, the value of β for the combined light from Pluto and Charon is 0.0372 ± 0.0016 (Tholen and Tedesco 1994). By combining the individual values for β and a_0 (mean brightness), a corresponding value of 0.0374 mag/deg is inferred for the system which closely matches the Tholen and Tedesco value.

A limited amount of color data was also taken. The F439W observations, transformed to Johnson B, provide resolved B–V colors at other than mutual event longitudes. To extract the color, each F439W observation was differenced against the nearest F555W measurement after correcting for the small difference in longitude between the pair of observations using the fitted lightcurve function. The B–V color for Charon is 0.710 ± 0.011 and shows no statistically significant change with longitude. The color for Pluto varies by a small amount; at $\lambda = 123°$, B–V = 0.873 ± 0.002 and at $\lambda = 289°$, B–V = 0.863 ± 0.002. Both the Charon and the Pluto numbers are consistent with previous mutual event measurements by Binzel (1988) and Reinsch *et al.* (1994). Even the variation seen on Pluto is consistent. The uncertainties on the Pluto color from mutual event observations are similar in size to our observed variation. The color variation indicates that Pluto is slightly redder at minimum light.

DISCUSSION

Lightcurves

The lightcurve of Pluto in Fig. 3 continues to show the familar lightcurve shape known for the system. Minimum light on Pluto occurs at $\lambda = 100°$ which is on its trailing hemisphere. Maximum light occurs at $\lambda = 220°$, just 120° away. The amplitude of Pluto's lightcurve is 0.33 mag, compared to 0.28 mag for the combined system lightcurve. The range of hemispherically averaged geometric albedo is 0.49 to 0.66, assuming radii from Buie *et al.* 1992.

Charon's lightcurve as shown in Fig. 4 looks very different from Pluto's. The amplitude, 0.08 mag, is considerably less, indicating a lesser degree of large scale contrast on its surface than for Pluto. The lightcurve is characterized

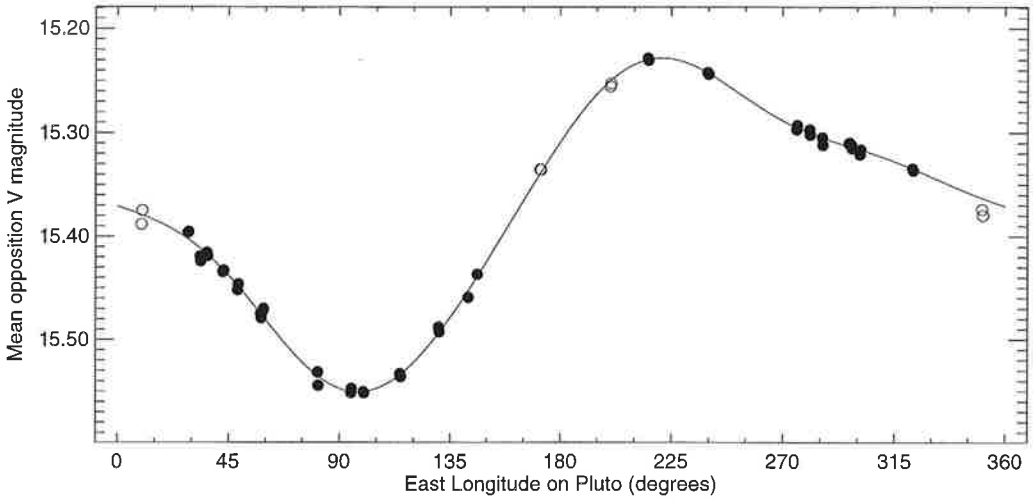

FIG. 3. Rotational lightcurve of Pluto. Mean opposition V magnitude $V(\lambda)$ is plotted against the sub-Earth longitude on Pluto λ in degrees. The data have been corrected for the phase function. All error bars are smaller than the symbols and are therefore not shown. Open circles indicates points not included in the fit. The solid curve represents the best-fit Fourier series.

by a minimum near $\lambda = 170°$, which is on the hemisphere of Charon pointed away from Pluto. The fitted lightcurve function formally has two local maxima at 50° and 280°, but looks more like a flat lightcurve away from the minimum. Unlike Pluto, Charon does not exhibit a strong peak in its lightcurve. The hemispherically averaged geometric albedo for Charon ranges from 0.36 to 0.39.

We can compare the Charon minus Pluto magnitude difference between the new lightcurves and the previous mutual event photometry. Lightcurves from Charon total eclipses show a depth of 0.17 mag (Tholen *et al.* 1987). This event depth implies a magnitude difference of 1.9 mag, which is in excellent agreement with the new lightcurves.

Phase Coefficients

When discussing the photometric variations versus solar phase angle, there are two distinct behaviors to keep in mind. The first is a linear increase in the magnitude of the object with decreasing phase angle. Many objects begin to

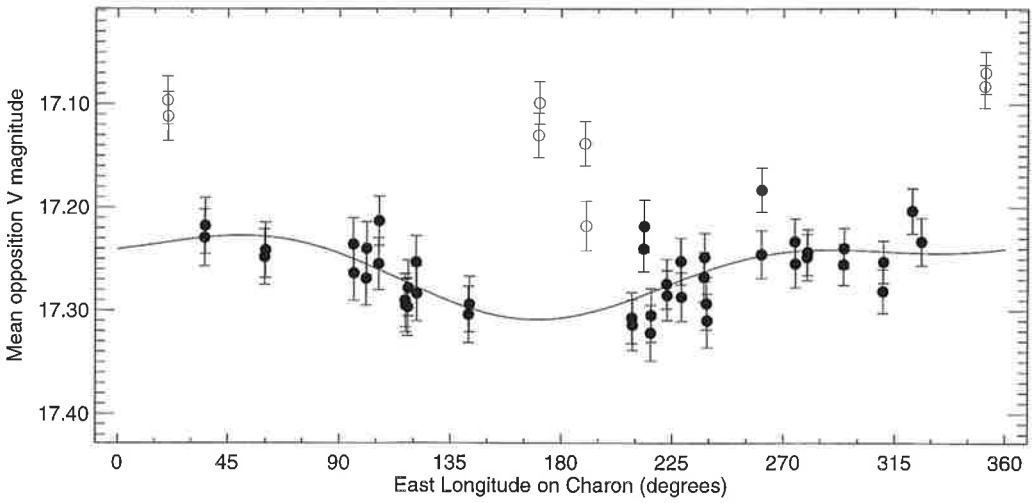

FIG. 4. Rotational lightcurve of Charon. Mean opposition V magnitude $V(\lambda)$ is plotted against the sub-Earth longitude on Charon λ in degrees. The data have been corrected for the phase function. Open circles indicates points not included in the fit. The solid curve represents the best-fit Fourier series.

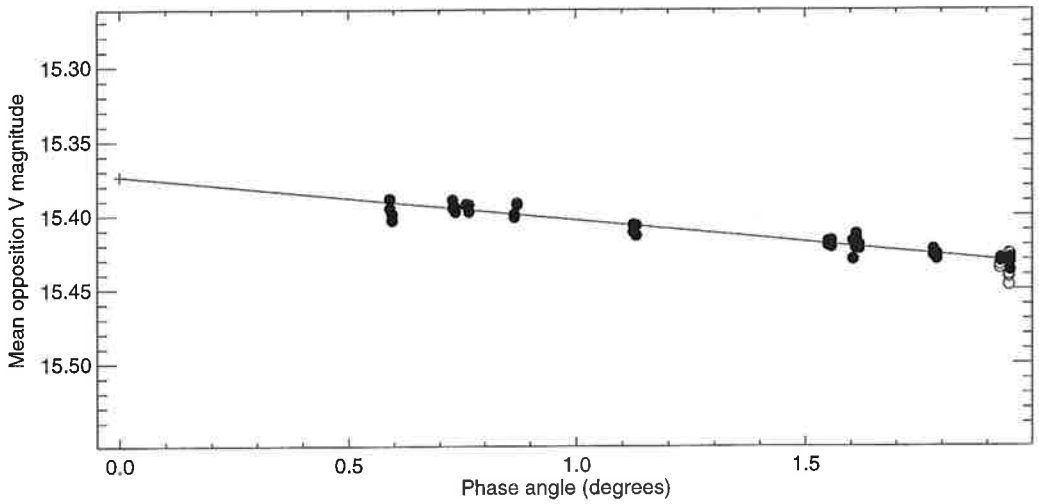

FIG. 5. Phase function for Pluto. Mean opposition V magnitude $V(\alpha)$ is plotted against phase angle α. The data have been corrected for the rotational lightcurve. The plus sign represents the intercept, $V_0 = 15.3735$. The solid line represents the fitted linear trend.

depart from this linear increase at some small phase angle, typically about 6° and show an additional nonlinear brightening that appears more quadratic in nature. We refer to the linear component as the opposition *effect* and the nonlinear trend as the opposition *surge*.

The phase coefficients we derive for Pluto and Charon are quite different but neither object exhibits an opposition surge. Compared to the mean system value, 0.0372 ± 0.0016, our results indicate that Pluto's phase variation is even smaller at 0.0294 ± 0.0011 mag/deg and Charon's phase effect is much larger at 0.0866 ± 0.0078 mag/deg. Table V provides a limited comparison of these newly derived linear phase coefficients with other objects in the Solar System over a similar phase angle range. Tabulated are values for the geometric albedo (p_v), linear phase coefficient (β), range of phase angle over which β was determined, a comment describing the photometric behavior at small phase angle, and finally a reference for the phase angle data. Where possible and necessary, we rederived a linear phase coefficient over a more limited range of phase angles so the number would be more closely comparable to the Pluto and Charon data. Figure 7 is a graphical representation of the information in Table V. The symbols next to the object name in the table match the symbol used in

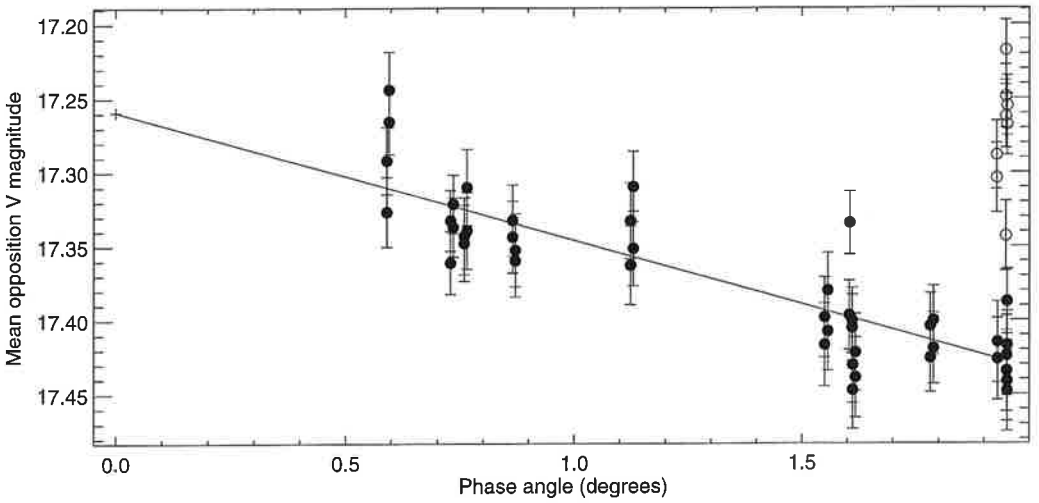

FIG. 6. Phase function for Charon. Mean opposition V magnitude $V(\alpha)$ is plotted against phase angle α. The data have been corrected for the rotational lightcurve. The plus sign represents the intercept, $V_0 = 17.2591$. The solid line represents the fitted linear trend.

TABLE III
Lightcurve Coefficients for Pluto

n	a_n	σ_a	b_n	σ_b
0	15.3735	0.0022	—	—
1	+0.0258	0.0010	+0.1284	0.0005
2	−0.0389	0.0014	−0.0348	0.0005
3	+0.0050	0.0008	−0.0012	0.0006
4	+0.0054	0.0010	−0.0019	0.0008
	$\beta =$	0.0294 ± 0.0011 mag/deg		
	$\chi^2_{red} =$	4.3		
	$\overline{\lvert O-C \rvert} =$	0.003 mag		

the figure. With the exception of Titan and Anchises, all these objects follow a general trend of lower β with higher geometric albedo.

The objects in the top half of the table (asterisks in plot) all exhibit typical phase variations with opposition surges for $\alpha < 6°$. The values for β all come from forcing a linear fit to the restricted range of phase angles. In all cases, there is clearly a nonlinear trend in the data that a linear fit does not follow. The fitted values for Tethys and Dione may be too small because they include data from a slightly larger range of phase angles.

The middle of the table lists examples of objects that do not show an opposition surge between 0.5° and 2.0°. Three possibilities exist to explain the lack of a surge: (1) the width of the opposition surge is narrower than the smallest observed phase angle, (2) the surge is very broad and appears linear over the small range of phase angles observed, or (3) there truly is no surge for the object. Titania and Oberon are excellent examples of case 1 where the surge is seen only inside 0.5°. If the surfaces of Pluto and Charon are similar then we may well be missing the surge altogether. By analogy with the uranian satellite data, we may have to wait until after 2004 to see the phase angle drop below 0.3°, where we may be able to begin detecting a surge. Observations at extremely small phase angles will have to wait for Pluto's ecliptic plane crossing in 2018. Case 3 may very well be impossible for solid surfaces. Only Titan may be exempt from an opposition surge altogether.

TABLE IV
Lightcurve Coefficients for Charon

n	a_n	σ_a	b_n	σ_b
0	17.2591	0.0116	—	—
1	−0.0334	0.0081	+0.0005	0.0050
2	+0.0148	0.0077	−0.0083	0.0057
	$\beta =$	0.0866 ± 0.0078 mag/deg		
	$\chi^2_{red} =$	1.3		
	$\overline{\lvert O-C \rvert} =$	0.019 mag		

TABLE V
Comparison of Photometric Properties in the Outer Solar System

Object	p_v	β	$\alpha(°)$	Small α	Reference
* 1 Ceres	0.10	0.09	0.5-2.0	surge	Tedesco *et al.*, 1983a
* 16 Psyche	0.10	0.07	0.5-2.0	surge	Tedesco *et al.*, 1983b
* 44 Nysa	0.49	0.076	0.5-2.0	surge	Harris *et al.*, 1989
* Io	0.6	0.07	0.5-2.0	surge	Veverka, 1977
* Europa	0.6	0.04	0.5-2.0	surge	Veverka, 1977
* Ganymede	0.4	0.05	0.5-2.0	surge	Veverka, 1977
* Callisto	0.2	0.09	0.5-2.0	surge	Veverka, 1977
* Tethys	0.78	0.020	0.3-6.3	surge	Franz and Millis, 1975
* Dione	0.65	0.033	0.5-6.3	surge	Franz and Millis, 1975
* Iapetus (bright)	0.5/0.04	0.06	0.5-2.0	surge	Franklin and Cook, 1974
• 1173 Anchises	0.03	0.023	0.3-2.0	no surge	French, 1987
• Rhea	0.55	0.023	0.5-6.4	no surge	Noland *et al.*, 1974
• Titan	0.2	0.005	0.3-6.4	no surge	Noland *et al.*, 1974
◇ Titania	0.23	0.066	0.5-3.0	surge <0.5	Goguen *et al.*, 1989
◇ Oberon	0.20	0.075	0.5-3.0	surge <0.5	Goguen *et al.*, 1989
• Triton	0.73	0.03*	0.05-1.7	no surge	Goguen *et al.*, 1989
• Pluto	0.51-0.71	0.029	0.6-2.0	no surge	this work
• Charon	0.38	0.087	0.6-2.0	no surge	this work

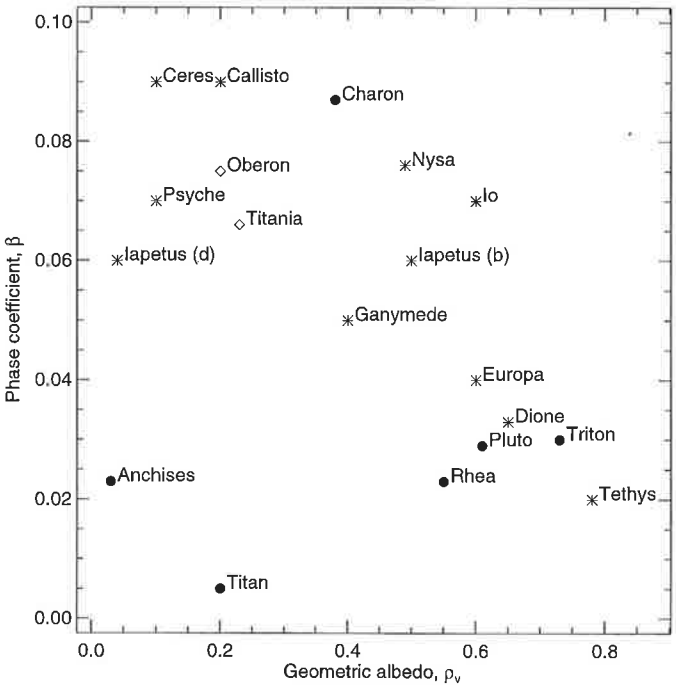

FIG. 7. Phase function comparisons. This figure is a graphical representation of the information in Table V. All objects plotted with an asterisk exhibit an opposition surge over the restricted range of phase angles. Objects that do not show a surge are plotted with filled circles. Objects plotted with open boxes have a surge that is confined to phase angles smaller than the restricted range.

Case 2 is more problematic and can be discarded only with very accurate photometry. Anchises (low-albedo Trojan asteroid) appears to have very unusual properties in that it has a similar phase coefficient to Pluto but it has a much lower albedo. If anything can be concluded from these comparisons, it would be that the phase coefficients of Pluto and Charon are consistent with other objects in the Solar System. Though they are quite different from each other, these new phase coefficients are not at all unusual.

Our vastly improved knowledge of the individual phase coefficients will be very useful in future analyses of mutual event observations. Until now, all work has been forced to assume identical photometric properties for Pluto and Charon. Over the possible range of phase angles the depth of a superior event (total occultation of Charon) can vary by as much as 0.01 mag in V, which would be noticeable in most of the photometry we have collected. There may well be a significant change in the radii inferred from the mutual event data once these new photometric properties are included.

Colors

The colors we derive are very consistent with previous mutual event results. Binzel (1988) derived $B-V$ of 0.867 ± 0.008 and 0.700 ± 0.010 for Pluto and Charon, respectively. Reinsch *et al.* (1994) found $B-V = 0.871 \pm 0.014$ and 0.701 ± 0.014 in close agreement with Binzel. Both sets of numbers represent color measurements of the anti-Charon hemisphere of Pluto ($\lambda = 180°$) and the Pluto-facing hemisphere of Charon ($\lambda = 0°$). Our results of 0.710 ± 0.011 for Charon at $\lambda = 123°$ and 289° are also consistent and provide evidence that there are no large scale color variations on the satellite. This property of Charon has been assumed in modeling mutual event photometry and is now validated.

Our colors for Pluto of $B-V = 0.873 \pm 0.002$ at $\lambda = 123°$ and $B-V = 0.863 \pm 0.002$ at $\lambda = 289°$ are also consistent with previous results. However, our two measurements do indicate a small difference in color with longitude on Pluto. This variation is quite small but does indicate that the darker regions on Pluto are more reddish in color. A globally uniform color of Pluto has also been assumed in most mutual event analyses but the amount of variation we see will cause very little change in the results derived.

CONCLUSIONS

Our new observations reveal individual photometric properties of Pluto and Charon. The lightcurve for Charon is seen to be small, thus confirming a common assumption used in lightcurve modeling. As has been often suspected, the shape of the lightcurve for the system is due to photometric variations from Pluto. The weak photometric phase variation and the reddish color are also seen to originate from Pluto. The difference in color between Pluto and Charon had been seen from mutual event observations, but this conclusion can now be extended globally.

These new measurements will be useful in improving the surface albedo maps of Pluto and Charon. From these photometric properties, the light contibution from Charon can now be cleanly removed leaving Pluto to be modeled directly. Convincing and accurate maps are critically needed, as shown in the companion paper (Tholen and Buie 1994), where the eccentricity of the orbit of Charon is seen to depend heavily on albedo distribution. Another promising step in future mapping efforts will be ultimately placing limits on or outright detection of albedo variability with time on the surface of Pluto. Completion of the next stage in mapping is beyond the scope of this work but remains a high priority for future investigations.

These observations should also help with planning a spacecraft mission to Pluto. A global view of the surface of Charon could be just as important in understanding the system as that of Pluto in providing important constraints on impactor fluxes when looking at Pluto's surface. Though Charon's lightcurve amplitude is small, there could very well be a difference between the area near minimum light (opposite Pluto) and the rest of the surface. Just as comparisons within the Earth–Moon system have led to numerous insights into the history of the Earth, we should expect to derive the same benefits from the study of the Pluto–Charon system. This distant binary planet may yet reveal the most interesting chapter yet in our understanding of the Solar System if we succeed in sending a spacecraft out for a visit.

ACKNOWLEDGMENTS

Profuse thanks to J. Holtzman for answering endless questions about WFPC and HST-OTA performance. Thanks to T. Lauer for bringing the CLEAN algorithm to our attention. This project also benefited a great deal from the programming assistance of Doug Loucks. Support for this work was provided by NASA through Grant GO-3848.01-91A from the Space Telescope Science Institute, which is operated by the Association of Universities for Research in Astronomy, Inc., under NASA Contract NAS5-26555. Additional support was provided to Tholen by NASA Grants NAGW 1991 and NAGW 3093.

REFERENCES

Binzel, R. P. 1988. Hemispherical color differences on Pluto and Charon. *Science* **241,** 1070–1072.

Binzel, R. P., and J. D. Mulholland 1984. Photometry of Pluto during the 1983 opposition: A new determination of the phase coefficient. *Astron. J.* **89,** 1759–1761.

Buie, M. W., and S. J. Bus 1992. Physical observations of (5145) Pholus. *Icarus* **100,** 288–294.

Buie, M. W., D. J. Tholen, and K. Horne 1992. Albedo maps of Pluto and Charon: Initial mutual event results. *Icarus* **97,** 211–227.

Buie, M. W., D. J. Tholen, and L. H. Wasserman 1994. Separate lightcurves of Pluto and Charon. *EOS* **75,** 216.

FRANKLIN, F. A., AND A. F. COOK 1974. Photometry of Saturn's satellites: The opposition effect of Iapetus at maximum light and the variability of Titan. *Icarus* **23,** 355–362.

FRANZ, O., AND R. L. MILLIS 1975. Photometry of Dione, Tethys, and Enceladus on the UBV system. *Icarus* **24,** 433–442.

FRENCH, L. M. 1987. Rotation properties of four L5 Trojan asteroids from CCD photometry. *Icarus* **72,** 325–341.

GOGUEN, J. D., H. B. HAMMEL, AND R. H. BROWN 1989. V photometry of Titania, Oberon, and Triton. *Icarus* **77,** 239–247.

HARRIS, A. W., J. W. YOUNG, L. CONTREIRAS, T DOCKWEILER, L. BELKORA, H. SALO, W. D. HARRIS, E. BOWELL, M. POUTANEN, R. P. BINZEL, D. J. THOLEN, AND S. WANG 1989. Phase relations of high albedo asteroids: The unusual opposition brightening of 44 Nysa and 64 Angelina. *Icarus* **81,** 365–374.

HARRIS, H. C., W. A. BAUM, D. A. HUNTER, AND T. J. KREIDL 1991. Photometry calibration of the *HST* Wide-Field/Planetary Camera. I. Ground-based observations of standard stars. *Astron. J.* **101,** 677–694.

HÖGBOM, J. 1974. Aperture synthesis with a non-regular distribution of interferometer baselines. *Astron. Astrophys. Supp.* **15,** 417–426.

JONES, J. H., C. A. CHRISTIAN, AND P. WADDELL 1988. Resolved CCD Photometry of Pluto and Charon. *Publ. Astron. Soc. Pac.* **100,** 489–495.

KEEL, W. C. 1991. A simple, photometrically accurate algorithm for deconvolution of optical images. *Publ. Astron. Soc. Pac.* **103,** 723–729.

MACKENTY, J. W., S. BAGGETT, J. BIRETTA, C. RITCHIE, AND W. SPARKS 1993. *WFPC Status and Performance Changes 1990–1993.* Proceedings from the Calibrating Hubble Space Telescope workshop, Baltimore, MD.

NOLAND, M., J. VEVERKA, D. MORRISON, D. P. CRUIKSHANK, A. R. LAZAREWICZ, N. D. MORRISON, J. L. ELLIOT, J. GOGUEN, AND J. A. BURNS 1974. Six-color photometry of Iapetus, Titan, Rhea, Dione and Tethys. *Icarus* **23,** 334–354.

OLKIN, C. B., L. A. YOUNG, J. L. ELLIOT, D. J. THOLEN, AND M. W. BUIE 1993. Individual light curves of Pluto and Charon. *Bull. Am. Astron. Soc.* **25,** 1132–1133.

RATNATUNGA, K. U., R. E. GRIFFITHS, S. CASERTANO, L. W. NEUSCHAEFER, AND E. W. WYCKOFF 1993. *Calibration of HST WFPC Images for Quantitative Analysis of Faint Galaxy Images.* Proceedings from the Calibrating Hubble Space Telescope workshop, Baltimore, MD.

REINSCH, K., V. BURWITZ, AND M. C. FESTOU 1994. Albedo maps of Pluto and improved physical parameters of the Pluto-Charon system. *Icarus* **108,** 209–218.

REITSEMA, H. J., F. VILAS, AND B. A. SMITH 1983. A charge-coupled device observation of Charon. *Icarus* **56,** 75–79.

TEDESCO, E. F., R. C. TAYLOR, J. DRUMMOND, D. HARWOOD, I. NICKOLOFF, F. SCALTRITI, H. J. SCHOBER, AND V. ZAPPALA 1983a. Worldwide photometry and lightcurve observations of 1 Ceres during the 1975–1976 apparition. *Icarus* **54,** 23–29.

TEDESCO, E. F., R. C. TAYLOR, J. DRUMMOND, D. HARWOOD, I. NICKOLOFF, F. SCALTRITI, AND V. ZAPPALA 1983b. Worldwide photometry and lightcurve observations of 16 Psyche during the 1975–1976 apparition. *Icarus* **54,** 30–37.

THOLEN, D. J., AND M. W. BUIE 1988. Circumstances for Pluto–Charon mutual events in 1989. *Astron. J.* **96,** 1977–1982.

THOLEN, D. J., AND M. W. BUIE 1997. The orbit of Charon. I. New Hubble Space Telescope observations. *Icarus* **125,** 245–260.

THOLEN, D. J., AND E. F. TEDESCO 1994. Pluto's lightcurve: Results from four oppositions. *Icarus* **108,** 200–208.

THOLEN, D. J., M. W. BUIE, AND C. E. SWIFT 1987. Circumstances for Pluto–Charon mutual events in 1988. *Astron. J.* **94,** 1681–1685.

VEVERKA, J. 1977. Photometry of satellite surfaces. In *Planetary Satellites* (J. A. Burns, Ed.), pp. 171–209. Univ. of Arizona Press, Tucson, AZ.

YOUNG, E. F., AND R. P. BINZEL 1993. Comparative mapping of Pluto's sub-Charon hemisphere: Three least squares models based on mutual event lightcurves. *Icarus* **102,** 134–149.